# Molecular Weight Distributions of Polyacrylamide by Photon Correlation Spectroscopy†

**Arthur DiNapoli and Ben Chu***

*Chemistry Department, State University of New York at Stony Brook, Long Island, New York 11794*

**Charles Cha**

*Calgon Corporation, Calgon Center, Pittsburgh, Pennsylvania 15230.*
*Received November 19, 1981*

ABSTRACT: We report a correlation function profile analysis of polyacrylamide samples with reasonably broad molecular weight distributions and show a comparison of results using different forms of the line width distribution function, $G(\Gamma)$, including the method of cumulants, Pearson's method, a histogram method, and $G(\Gamma) = \Gamma^{\nu-1}e^{-\alpha\Gamma}$, with $\alpha$ and $\nu$ being constants. The importance of the low-frequency (high molecular weight) limit in the transformation is emphasized. By realizing the sharp cutoff nature of the histogram approach, we find the Pearson method to be particularly applicable to unimodal but broad molecular weight distributions with long tails and the simple analytical forms of $G(\Gamma)$ to be feasible for qualitative discussions.

## I. Introduction

We have succeeded in obtaining either unimodal or bimodal line width distributions of arbitrary forms from a correlation function profile analysis.[1,2] The histogram method represents a practical and approximate solution to the ill-conditioned Laplace inversion problem. With sufficiently precise data of the time correlation function, we have tested this approach using simulated data, Dow latex spheres of known size distributions,[1,2] polystyrene in cyclohexane,[3] and poly[bis(*m*-chlorophenoxy)phosphazene] in chloroform.[4] As the histogram method uses a finite number of discrete steps and since truncation of tails in the line width distribution function is not a desirable approximation in some cases, we report an extension of our treatment on the determination of broad line width distributions with long tails and demonstrate our methods using two polyacrylamide samples whose characterization method is being developed.[5]

## II. Experimental Section

**1. Sample Preparation.** We purchased one polyacrylamide sample (PAM-A) from Polysciences (catalog no. 8248, lot no. 93-3). The molecular weight was reported as $2.5 \times 10^5$. A second, higher molecular weight sample (PAM-B) was prepared specifically for this study. The polymerization process was terminated after 10% conversion in order to obtain a narrower molecular weight distribution for comparison purposes.

Three sets of solutions were prepared. They are designated as solutions A, B, and C. Solution A consists of the Polysciences polymer dissolved in 0.5 N $NaNO_3$. A stock solution was prepared and then filtered (Millipore filter with a nominal pore diameter of 0.22 $\mu$m) directly into light scattering cells, diluted with filtered (Millipore, 0.10 $\mu$m) solvent, and flame sealed. Solutions B and C were Polysciences and Calgon polymers, respectively, dissolved in pure water. About 10 mL of the stock solution (~1% w/v) was prepared by dissolving the dry polymer in filtered (Millipore 0.05 $\mu$m), doubly distilled, deionized water. The solution was stirred gently overnight, transferred to clean, septum-capped light scattering cells without filtration, diluted to predetermined concentrations with filtered water, and allowed to equilibrate for 24 h. All measurements were completed within 24 h after equilibration. The cells were centrifuged at least 1 h at 7000*g* immediately prior to measurements. Although the polymer solution was never filtered, the samples were essentially dust free. Measurements were performed at 25.00 ± 0.01 °C.

**2. Light Scattering Measurements.** Measurements were performed with the spectrometer schematically shown in Figure 1. We used a Spectra-Physics Model 165 argon ion laser operating, normally, below 100 mW. Intensity measurements were accumulated automatically every 2.5° between the scattering angles, $\theta$, of 35° and 150° by gating the frequency counter 10 times at each angle for 1 s. The count values were averaged (any value greater than 10% (much greater than statistical counting errors) from the mean was discarded) and normalized by the voltage from the photodiode. For our samples, all 10 values were invariably within 10%; in fact, at each angle the three runs usually agreed to within 0.5%.

Correlation function measurements were made by routing the signal from the discriminator to the 96-channel, single-clipped Malvern correlator. In order to optimize the correlation signal, we used a 0.5-mm pinhole (instead of a slit for static measurements), thereby reducing the acceptance angle and creating a cross section in the neighborhood of one coherence area. Problems often arise in interpreting the correlation function profile when an extended, nonzero base line exists. Such a base line can sometimes be attributed to large dust particles or aggregates traversing the scattering volume and is in excess of the computed base line. Therefore, the net signal of interest is no longer the difference between the measured time correlation function and the computed base line. Our correlator has been modified to make a direct determination of the base line by introducing a delay of $320\Delta\tau$, where $\Delta\tau$ is the delay time increment between the 92nd and 93rd channel. If we let 92 channels cover about three characteristic decay times, a delay time of $320\Delta\tau$ between the 92nd and 93rd channel corresponds to measurements of the correlation function after about 13 characteristic decay times when the net signal has fallen to the background level. Four channels (93–96) were used to measure the time correlation function at $413\Delta\tau$, $414\Delta\tau$, $415\Delta\tau$, and $416\Delta\tau$ delay times. The values were averaged in order to improve the counting statistics. The measured and computed base lines always agree to within 1%, again indicating relatively dust-free and stable system operations.

If dust particles were present, the measured base line, which was the averaged value of the correlation function at very long delay times, could be substantially higher than the computed base line using information from the monitor channels of the correlator. Then we would discard the measurement and reexamine the sample preparation. Furthermore, we may introduce a delay between the 24th and 25th channels of up to 272 $\Delta\tau$ in increments of 64 channels. The second feature enables us to extend the number of channels beyond 96, as will be described.

In addition to the spectrometer shown in Figure 1, we have used a laboratory-built, low-angle instrument shown schematically in Figure 2. At $\theta \lesssim 20°$ we need only a small, helium–neon laser (Spectra-Physics Model 124) operating below 10 mW as our light source. The thick, high-quality glass disks keep the scattering from the glass–air interfaces (A) away from the sample volume, which is less than 1 mL. The micrometer stage allows us to move the scattering volume close to point B, which represents the source of our local oscillator due to the stray light from the liquid–glass

† Work supported by the Polymer Program, Division of Materials Research, National Science Foundation (Grant DMR 8016521).

0024-9297/82/2215-1174$01.25/0 

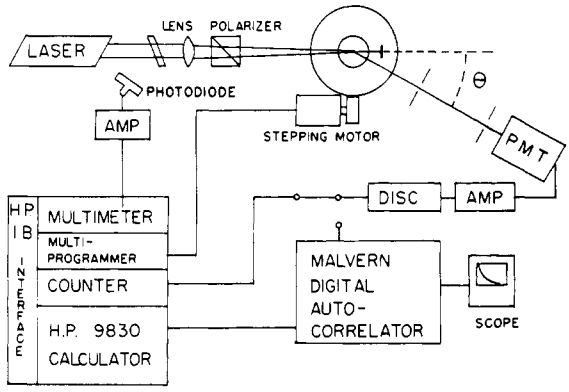


**Figure 1.** Schematic diagram of spectrometer for static and dynamic measurements between $\theta = 30°$ and $\theta = 150°$.

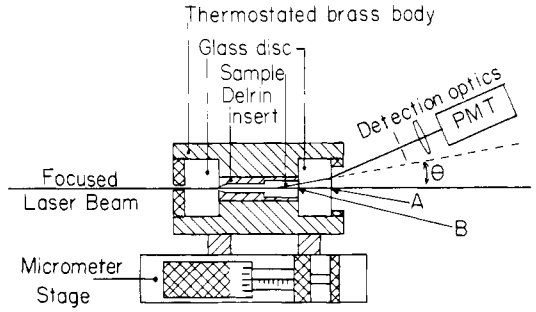


**Figure 2.** Schematic diagram of scattering cell for dynamic measurements below $\theta = 20°$.

interface, or deep into the sample chamber, where there is a minimum of stray light. In this way we may measure either the self-beating or homodyne correlation function. There is an incorrect but more widely used notation of identifying self-beating with homodyning and homodyning with heterodyning. In this article, we refer to self-beating of the scattered light without a local oscillator, homodyning of scattered light with a local oscillator of the same frequency as the incident light, and heterodyning of scattered light with a local oscillator of a shifted frequency different from that of the incident light.

The thermostated, brass body is a cylinder of 1-1/2 in. diameter × 4 in. length with a 1/2 in. diameter × 1 in. length Delrin insert to contain the solution. The insert is removable for easy cleaning and is carefully designed to allow for dust-free filling and to eliminate bubbles. However, since we cannot centrifuge the sample cell, it is usually necessary to filter the solutions.

**3. Gel Permeation Chromatography.** GPC measurements were done at Calgon using the Polysciences sample (PAM-A) with 0.5 N $NaNO_3$ as the solvent (sample A). The column was calibrated by measuring the elution volume of three polyacrylamide samples whose molecular weights had been determined with a Chromatix KMX laser scattering spectrometer. The resulting weight-fraction molecular weight distribution was then converted to a number-fraction molecular weight distribution.

## III. Data Analysis

**1. Intensity of Scattered Light.** The intensity data have been analyzed by using the classical Rayleigh–Gans–Debye equations in their limiting forms:

$$\lim_{\theta \to 0} \frac{HC}{R_{VV}} = \frac{1}{M_w} + 2A_2C \tag{1}$$

$$\lim_{C \to 0} \frac{HC}{R_{VV}} = \frac{1}{M_w} + \frac{3\lambda_0^2}{16\pi^2 n_0^2} \frac{1}{M_w} \langle r_g^2 \rangle_z \sin^2(\theta/2) \tag{2}$$

where $H = 4\pi^2(\partial n/\partial C)^2 n_0^2/N_A\lambda_0^4$, with $\partial n/\partial C$, $n_0$, $N_A$, and $\lambda_0$ being, respectively, the refractive index increment, the refractive index of the solvent, Avogadro's number, and the wavelength in a vacuum. $C$ is the concentration (w/v), $A_2$ is the second virial coefficient, and $M_w$ ($=\sum N_i M_i^2/\sum N_i M_i$, $N_i$ being the number of molecules with molecular weight $M_i$) is the weight-average molecular weight. $R_{VV}$, the absolute Rayleigh ratio, is determined from the measured, relative Rayleigh ratio, $R_{VV}$*, using the known Rayleigh ratio of benzene.[6] The value of $\partial n/\partial C$ has been measured with a Jena laboratory interferometer, giving, for sample B, 0.160 at $\lambda = 488.0$ nm.

We have determined the concentration-dependent radius of gyration from a plot of $HC/R_{VV}$ vs. $\sin^2(\theta/2)$ through the equation

$$\langle r_g^2(C) \rangle_z = \frac{\text{initial slope}}{\text{intercept}} \frac{3\lambda_0^2}{16\pi^2 n_0^2}(1 + 2A_2CM_w) \tag{3}$$

**2. Line Width Analysis.** The net, measured, self-beating correlation function for a polydisperse solution is given by

$$G_{net}^{(2)}(\tau) = A^*\beta \left| \int_0^\infty G(\Gamma) e^{-\Gamma\tau} \, d\Gamma \right|^2 \tag{4}$$

where $A^*\beta$ is the product of the base line and an instrumental constant that can be determined in the fitting procedure. $G(\Gamma)$ is the normalized line width distribution function, with $\Gamma$ being the line width and $\tau$, the delay time ($=\Delta\tau I$, where $I$ is the channel number). As we want to deduce the molecular weight distribution from the line width distribution, the form of $G(\Gamma)$ must be mathematically compatible with the transformation procedure, which we will describe in detail in a later section. However, it is appropriate to enumerate the requirements placed on the form of $G(\Gamma)$ at this time, since they will dictate the best means of extracting an estimate of $G(\Gamma)$ from the correlation function. Our general ideas can be summarized as follows:

(1) A continuous form of $G(\Gamma)$ for which the Laplace transformation, described by the integral in eq 4, can be carried out analytically is highly desirable. The continuous form of $G(\Gamma)$ is in addition to the Pearson and the Schulz distributions.

(2) The computed correlation function must agree with the measured one to within the statistical counting error limits.

(3) The mean line width and the normalized second moment of $G(\Gamma)$ should agree with values obtained by more established techniques, such as the cumulants method.

(4) The fitting procedure should not require excessive computer time for processing.

(5) We should not need an a priori knowledge of the shape of the distribution.

We have analyzed $G_{net}^{(2)}(\tau)$ in four different ways, none satisfying all of the above requirements but each having unique advantages. The first technique is the method of cumulants,[7] which is currently the most widely used technique for analyzing polydispersity effects. We expand the logarithim of the first-order field correlation function, $g^{(1)}(\tau)$ ($=\int_0^\infty G(\Gamma)e^{-\Gamma\tau} \, d\Gamma$) about the mean line width and obtain

$$g^{(1)}(\tau) \simeq \exp\left\{-\bar{\Gamma}\tau + \sum(-1)^i \frac{\mu_i \tau^i}{i!}\right\} \tag{5}$$

where

$$\bar{\Gamma} = \int_0^\infty \Gamma G(\Gamma) \, d\Gamma \tag{6}$$

and

$$\mu_i = \int_0^\infty (\Gamma - \bar{\Gamma})^i G(\Gamma) \, d\Gamma \tag{7}$$

The approximations used in obtaining eq 5 require small $\tau$ values. When $\bar{\Gamma}\tau_{max}$ is less than 0.5, we need only one term of the summation in eq 5 where $\tau_{max}$ is the $\tau$ value at the last correlator channel. As $\bar{\Gamma}\tau_{max}$ increases to 4, $i$ must increase to 5 or 6. In order to obtain information on the correlation function profile, we need to measure four or five correlation functions using various values of $\bar{\Gamma}\tau_{max}$, fit each data set using different values of $i$, and extrapolate the results to zero delay time. In the cumulants approach, we do not obtain $G(\Gamma)$, but rather the moments of the distribution. Therefore, this technique is of little utility if we want to determine the molecular weight distribution, $f(M)$, from light scattering measurements. While the moments of $G(\Gamma)$ can be used to estimate the moments of $f(M)$ for narrow distributions,[8] we use them only to verify the results by other techniques.

The second method of analysis is the histogram technique, which has been described[1,2] and utilized[3,4] elsewhere. The integral in $g^{(1)}(\tau)$ is approximated by a series of $L$ histograms, as described by

$$g^{(1)}(\tau) = \sum_{i=1}^{L} G(\Gamma_i) \int_{\Gamma_i-\Delta\Gamma/2}^{\Gamma_i+\Delta\Gamma/2} \exp(-\Gamma\tau)\, d\Gamma \qquad (8)$$

This method approximates $G(\Gamma)$ using a series of discrete steps, each with a step width $\Delta\Gamma$. $\bar{\Gamma}_i$ is the arithmetic center of step $i$. In our experiments, the value of $L$ can be as high as 10 for the most precise data. Although the same nonlinear least-squares algorithm, due to Marquadt,[9] is used in this approach as in the method of moments, it is used in an interactive way, which makes greater demands of the programmer. Our technique accommodates bimodal distributions easily,[9,10] while other methods[1] fail. The means and moments of the histogram distribution are computed through

$$\bar{\Gamma} = \frac{\sum_{i=1}^{L} \frac{G(\Gamma_i)}{2}\left\{\left(\bar{\Gamma}_i + \frac{\Delta\Gamma}{2}\right)^2 - \left(\bar{\Gamma}_i - \frac{\Delta\Gamma}{2}\right)^2\right\}}{\sum_{i=1}^{L} G(\Gamma_i)\Delta\tau} \qquad (9)$$

$$\mu_k = \frac{\sum_{i=1}^{L} \frac{G(\Gamma_i)}{k+1}\left\{\left(\bar{\Gamma}_i - \bar{\Gamma} + \frac{\Delta\Gamma}{2}\right)^{k+1} - \left(\bar{\Gamma}_i - \bar{\Gamma} - \frac{\Delta\Gamma}{2}\right)^{k+1}\right\}}{\sum_{i=1}^{L} G(\Gamma_i)\Delta\Gamma} \qquad (10)$$

Our third approach has been to arbitrarily choose a simple function[11] for which the Laplace transformation is analytical:

$$G(\Gamma) = \Gamma^{\nu-1}e^{-\alpha\Gamma}$$

$$g_N^{(1)}(\tau) = \gamma(\tau + \alpha)^{-\nu} \qquad (11)$$

where $\gamma$ is the gamma function and $g_N^{(1)}(\tau)$ indicates that we normalize the correlation function before fitting it to eq 11. Since this function is only a two-parameter fit, the calculations can be performed efficiently on a Hewlett-Packard desk top calculator (9830A). The mean and second moment for eq 11 are

$$\bar{\Gamma} = [\gamma(\nu + 1)/\gamma(\nu)]/\alpha$$

$$\mu_2/\bar{\Gamma}^2 = \{\gamma(\nu + 2)\gamma(\nu)/[\gamma(\nu + 1)]^2\} - 1 \qquad (12)$$

Our fourth approach has been to assume $G(\Gamma)$ to have a Pearson-type distribution:

$$G(\Gamma) = A(\Gamma/B - 1)^C(1 - \Gamma/D)^E \qquad (13)$$

where $A$ represents a normalization factor, $B$ and $D$ fix the upper and lower limits of $G(\Gamma)$, respectively, and $C$ and $E$ determine the shape of the distribution. Numerical integrations are required at each of the 92 data points, as well as for the derivative of $G(\Gamma)$ with respect to four of the five fitting parameters. In order to fit one correlation function, one must perform over 10 000 numerical integrations of 150 increments each, making this method the most demanding in terms of computer time. We have used both a cubic spline integration[12] and Simpson's rule with similar results. Values of $\bar{\Gamma}$ and $\mu_i$ are also determined by numerical integration.

Table I
Results of Intensity Measurements for Three Samples

| sample | $M_w \times 10^5$ | $\langle r_g^2\rangle_z^{1/2}$,[a] Å | $A_2 \times 10^{-4}$, (mL·mol)/g² |
|---|---|---|---|
| A | 2.2 ± 0.9 | 250 ± 25 | 4.3 ± 0.2 |
| B | 2.6 ± 0.1 | 320 ± 20 | 3.9 ± 0.2 |
| C | 4.6 ± 0.1 | 415 ± 20 | 3.9 ± 0.2 |

[a] From Zimm plots.

Table II
Comparison of Cumulants and Histogram Techniques for Sample A

| | | cumulants | | histograms | |
|---|---|---|---|---|---|
| $C$, wt % | $\theta$, deg | $\bar{\Gamma} \times 10^3$, rad/s | $\mu_2/\bar{\Gamma}^2$ | $\bar{\Gamma} \times 10^3$, rad/s | $\mu_2/\bar{\Gamma}^2$ |
| 0.4 | 60 | 4.99 | 0.35 | 5.00 | 0.53 |
| 0.198 | 90 | 9.82 | 0.25 | 9.26 | 0.32 |
| 0.198 | 60 | 4.35 | | 4.42 | 0.35 |
| 0.098 | 60 | 4.30 | 0.36 | 4.32 | 0.44 |
| 0.05 | 60 | 4.20 | 0.30 | 4.23 | 0.37 |

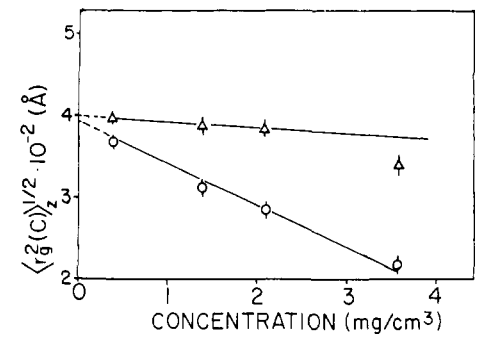


**Figure 3.** Plot of $\langle r_g^2(C)\rangle_z^{*1/2}$ (○) and $\langle r_g^2(C)\rangle_z^{1/2}$ (△) vs. concentration for sample C. Extrapolation of $\langle r_g^2(C)\rangle_z^{1/2}$ [$=\langle r_g^2(C)\rangle_z^{*1/2}(1 + 2A_2CM_w)$] to zero concentration gives $\langle r_g^2(C \to 0)\rangle_z^{1/2}$ = 400 Å.

## IV. Results

**1. Intensity Measurements.** Results for the three sample solutions are tabulated in Table I. A plot of the radius of gyration vs. concentration is given for sample C in Figure 3.

**2. Cumulants Analysis.** As noted previously, the cumulants technique yields only $\bar{\Gamma}$ and $\mu_2/\bar{\Gamma}^2$ reliably and is therefore not of use in determining $f(M)$. We have done the analysis only for sample A to show that both the cumulants and the histogram techniques give similar $\bar{\Gamma}$ and $\mu_2/\bar{\Gamma}^2$ values, provided that appropriate terms are used in the cumulants expansion technique. Table II presents this comparison and Figure 4 shows a typical cumulants extrapolation. Due to the ambiguity of the extrapolations, we have taken the histogram values to be more reliable and will use them throughout this work as a measure of the true values of $\bar{\Gamma}$ and $\mu_2/\bar{\Gamma}^2$.

**3. Histograms.** In performing the histogram fits, we often found a bimodal form of $G(\Gamma)$, as shown in Figure 9a. For polyacrylamides, a bimodal molecular weight

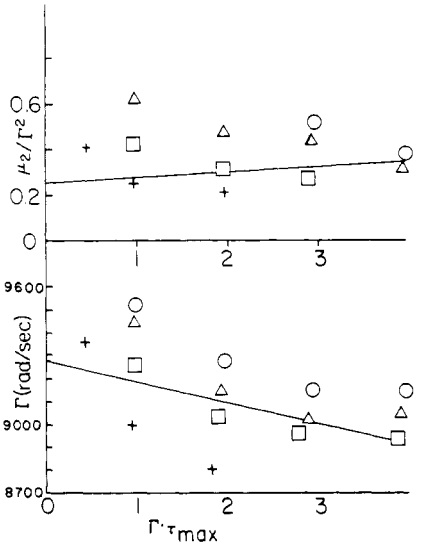


**Figure 4.** Cumulants extrapolation for sample A, $C = 0.098$ wt %, $\theta = 90°$: $i = 2$ (+), $i = 3$ (□), $i = 4$ (△), and $i = 5$ (○), where $i$ refers to the index in eq 5. A correct extrapolation of $\bar{\Gamma}$ and $\mu_2/\bar{\Gamma}^2$ to $\bar{\Gamma}\tau_{max} = 0$ is ambiguous because the range of applicability of different order cumulant fits in $\bar{\Gamma}\tau_{max}$ is limited and varies with the nature of $G(\Gamma)$. The straight lines are drawn to show that higher order cumulant fits are needed with increasing $\bar{\Gamma}\tau_{max}$.

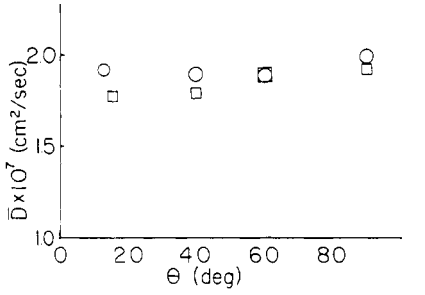


**Figure 5.** $\bar{D}$ vs. $\theta$ for sample B: $C = 0.492$ wt % (○) and $C = 0.718$ wt % (□).

distribution is chemically unreasonable, and the unimodal character of the GPC elution profile supports this conclusion. A pseudogel behavior is known to manifest itself as a high-frequency peak in the histogram[13] but the molecular weight and the concentration are too low to account for the apparent bimodal behavior, even for a gel-forming polymer such as polyacrylamide. One approach to detect the pseudogel behavior is to measure the diffusion coefficient as a function of scattering angle ($\theta$). As $\theta$ increases, we probe shorter range interactions and ths pseudogel behavior should become apparent as an increase in the measured diffusion coefficient over its translational diffusion coefficient value obtained at low scattering angles. The results of this experiment are shown in Figure 5, where $\bar{D} = \bar{\Gamma}/K^2$ and $K = 4\pi \sin(\theta/2)/\lambda$.

At $\theta \lesssim 20°$ we used the low-angle cell and analyzed the results according to

$$G_{net}^{(2)}(\tau) = A^*\beta(c_1 g^{(1)}(\tau) + c_2|g^{(1)}(\tau)|^2) \qquad (14)$$

where $c_1$ and $c_2$ are functions of the number of photocounts due to stray light ($n_{10}$) and scattered light ($n_s$). For $n_{10} \gg n_s$, $c_1 \gg c_2$ and for $n_s \gg n_{10}$, $c_2 \gg c_1$. When the stray light dominates the signal observed by the photomultiplier, a condition which is easy to verify experimentally, we measure the homodyne correlation function. We have attempted to exclude all the stray light and measure the pure self-beating correlation function at fairly small scattering angles. We can never be sure that $c_2$ dominates completely, and consequently, these fits have larger errors.

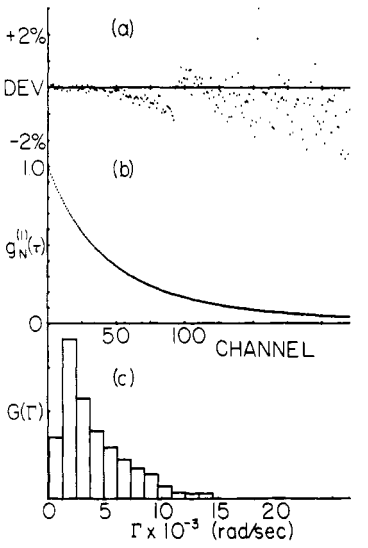


**Figure 6.** Results of line width analysis using three separate measured correlation functions for sample B, $\theta = 60°$, $C = 0.215$ wt %. Shown are the deviation $[g^{(1)}(\tau)_{measd} - g^{(1)}(\tau)_{computed}]/g^{(1)}(\tau)_{measd} \times 100$ (a), $g_N^{(1)}(\tau)$ after overlapping the three sets of data (b), and the line width histogram (c).

For sample B, the 12° data point for the 0.492 wt % solution represents a homodyne fit and the 17° point for the 0.718 wt % solution represents a self-beating fit. From low-angle line width data we can rule out the pseudogel behavior. Thus, we conclude that the bimodal character is an artifact of the histogram technique for broad distributions with long tails. It arises because the high-frequency tail of the histogram has very low values of $G(\Gamma_i)$.

We have also constructed a 220-point correlation function using the modified 96-channel correlator by measuring three correlation functions with a delay of $0 \times 64 \times \Delta\tau$, $1 \times 64 \times \Delta\tau$, and $2 \times 64 \times \Delta\tau$ between channels 24 and 25. Since we can normalize each correlation function by its measured base line and compare the channels with identical $\tau$ values, we can overlap the separately measured correlation functions and create a 220-point correlation function.

The three measured correlation functions with delays of $0 \times 64 \times \Delta\tau$, $1 \times 64 \times \Delta\tau$, and $2 \times 64 \times \Delta\tau$ between channels 24 and 25 represent correlation functions with delay channels (a) 1–24, 25–92, and 413–416, (b) 1–24, 89–156, and 477–480, and (c) 1–24, 153–220, and 541–544. The agreement in the base lines (413–416, 477–480, and 541–544) and the initial 24 channels suggests whether overlaps are within statistical error limits. Three net correlation functions after subtraction of the individually measured base lines are then scaled by using values of the first 24 channels. Ratios of the overlaps for channels 89–92 between correlation functions a and b and those for channels 153–156 between correlation functions b and c should be constants within the statistical counting error limits. Such a procedure requires high accumulation and, therefore, very stable long-term characteristics of the spectrometer. The results for sample B at $\theta = 60°$ and $C = 0.215$ wt % show a unimodal distribution, with $\bar{D} = 1.38 \times 10^{-7}$ cm²/s. The combined correlation function, the deviation of the measured and computed results, and the deduced histogram are shown in Figure 6, while the 96-channel fit gives a pseudobimodal distribution, with $\bar{D} = 1.41 \times 10^{-7}$. We take this as further evidence that the line width distribution is truly unimodal.

In order to perform the transformation of $G(\Gamma) \rightarrow f(m)$, we need the value of $k_D$, defined by

$$D \approx D_0(1 + k_D C) \qquad (15)$$

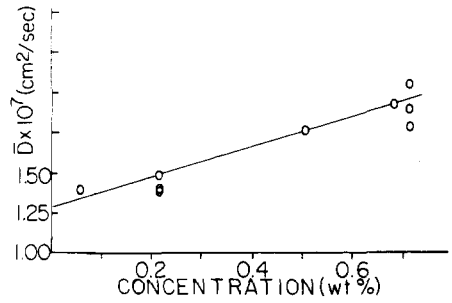


**Figure 7.** $\bar{D}$ vs. concentration for sample B. $k_D$ = 72 g/g, $\bar{D}_0$ = (1.29 ± 0.05) × $10^{-7}$ $cm^2/s$.

Table III
Results of Fitting Line Width Data to Eq 11 for Sample C[a]

| $C$, wt % | $\theta$, deg | $\alpha \times 10^4$, s | $\nu$ | $\bar{\Gamma} \times 10^3$,[b] $s^{-1}$ | $\mu_2/\bar{\Gamma}^2$ |
|---|---|---|---|---|---|
| 0.21 | 60 | 7.6 ± 0.1 | 3.06 ± 0.05 | 4.00 (±2%) | 0.33 (±2%) |
| 0.04 | 90 | 6.2 ± 0.4 | 4.3 ± 0.2 | 7.00 (±6%) | 0.23 (±5%) |

[a] From a histogram fit: $\bar{\Gamma}(\theta = 60°, C = 0.21$ wt %) = 3.90 × $10^3$ $s^{-1}$; $\bar{\Gamma}(\theta = 90°, C = 0.04$ wt %) = 6.90 × $10^3$ $s^{-1}$. [b] A range of values that gave reasonable fits was obtained. The percent deviations reflect the spread of acceptable results.

We first compute $\bar{D}$ using the histogram analysis, plot $\bar{D}$ vs. $C$, and then obtain $\bar{D}_0$ and $k_D$ from the intercept and slope as shown in Figures 7 and 8.

**4. Simple Forms of $G(\Gamma)$.** Results of our analysis using eq 11 for sample C are given in Table III. A serious problem in this approach is that $G(\Gamma)$ remains finite in the very low frequency region. We tried to compensate this weakness by arbitrarily setting the lower limit of the integration at $\Gamma_{min}$, performing a numerical integration from $\Gamma = 0$ to $\Gamma_{min}$, and subtracting the results from $G(\Gamma)$ computed from $\Gamma = 0$. The results, judging by a deviation plot, are slightly improved. However, the additional integration nullifies the simplicity for which we have chosen eq 11.

**5. Pearson's Fit.** The results from sample A at $C$ = 0.098 wt % and $\theta = 60°$ are shown in Figure 9b. In order to improve the resolution at the lower frequencies, we applied Simpson's rule independently above and below the value of $\Gamma$ where $G(\Gamma)$ exhibits a maximum. We chose 150 integration steps over the entire range of $G(\Gamma)$, a value we found to be optimal, and set the fraction of those steps below $G_{max}(\Gamma)$ to be 0.3–0.4 of the total number of steps. The method permits a much narrower step size below $G_{max}(\Gamma)$, resulting in an improved deviation plot.

Deviation plots for the distributions of Figure 9 are shown in Figure 10. The results are typical. The histogram $G(\Gamma)$ yields $G_{net}^{(2)}(\tau)$ that are in agreement with the measured $G_{net}^{(2)}(\tau)$ to within 1% and the Pearson fit yields errors that may exceed 2% at the highest channels. The deviation plot shown in Figure 10 is actually only of the marginal quality. Most Pearson fits have deviation plots resembling Figure 10a. Table IV gives numerical values of fits by the Pearson equation, while Table V compares

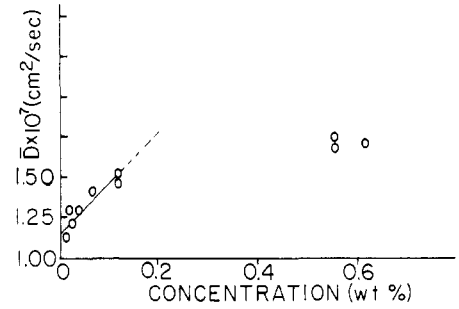


**Figure 8.** $\bar{D}$ vs. concentration for sample C. $k_D$ = 277 g/g, $\bar{D}_0$ = (1.15 ± 0.10) × $10^{-7}$ $cm^2/s$. Equation 15 is valid only in dilute solutions. At $C \gtrsim 0.6$ wt %, higher order coefficients need to be taken into account.

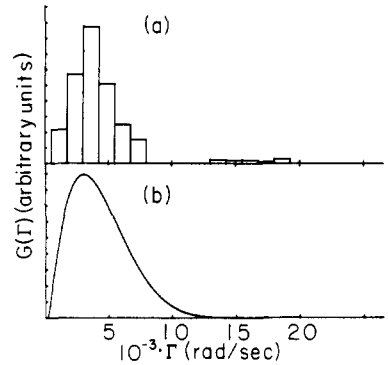


**Figure 9.** $G(\Gamma)$ vs. $\Gamma$ for sample A, $C$ = 0.098 wt %, $\theta = 60°$, using histograms (a) and Pearson's fit (b).

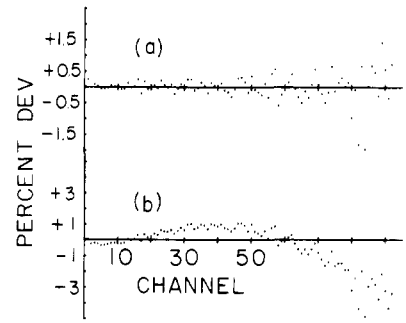


**Figure 10.** Deviation plots for distributions given in Figure 9. (a) and (b) refer to the same fits as in Figure 9. DEV = $[g^{(1)}(\tau)_{measd} - g^{(1)}(\tau)_{computed}]/g^{(1)}(\tau)_{measd}$ (%).

values of $\bar{\Gamma}$ and $\mu_2/\bar{\Gamma}^2$ for different samples using the histogram and Pearson fits.

**6. Molecular Weight Transformation.** By assuming that the only contribution to the line width distribution is due to the translational motion of polymer molecules of different sizes, we can transform the distribution of diffusion coefficients to the molecular weight distribution. First, the line width distribution is transformed in a straightforward way to the distribution of diffusion coefficients $G(D)$ corrected to infinite dilution using

$$D_0 = D/(1 + k_D C) = \Gamma/K^2(1 + k_D C) \qquad (16)$$

Table IV
Numerical Values for Parameters in the Pearson Fits

| sample | $C$, wt % | $\theta$, deg | $A$ | $B$[a] | $C$[a] | $D$ | $E$ |
|---|---|---|---|---|---|---|---|
| A | 0.098 | 60 | 9.01 × $10^{-3}$ | 1325 | 0.299 | 22 670 | 7.89 |
| B | 0.057 | 90 | 4.44 × $10^{-4}$ | 1390 | 0.795 | 14 800 | 4.42 |
| B | 0.226 | 90 | 2.81 × $10^{-4}$ | 3830 | 0.518 | 34 210 | 2.81 |
| C | 0.0116 | 60 | 3.78 × $10^{-4}$ | 3100 | 0.574 | 21 380 | 7.32 |
| C | 0.1147 | 90 | 7.50 × $10^{-4}$ | 1150 | 0.522 | 27 869 | 2.94 |

Table V
Comparisons of the Mean and Normalized Second Moments Obtained Using Different Fits

| sample | θ, deg | C, wt % | histogram fit $\bar{\Gamma} \times 10^3$, $s^{-1}$ | histogram fit $\mu_2/\bar{\Gamma}^2$ | Pearson's fit $\bar{\Gamma} \times 10^3$, $s^{-1}$ | Pearson's fit $\mu_2/\bar{\Gamma}^2$ |
|---|---|---|---|---|---|---|
| A | 60 | 0.098 | 4.33 | 0.44 | 4.29 | |
| B | 90 | 0.057 | 8.56 | 0.43 | 8.54 | 0.25 |
| B | 90 | 0.226 | 10.9 | 0.46 | 10.2 | 0.33 |
| C | 40 | 0.012 | 1.54 | 0.3 | | |
| C | 60 | 0.012 | 3.31 | 0.31 | 3.46 | 0.42 |
| C | 90 | 0.115 | 8.56 | 0.52 | 8.63 | 0.26 |
| C | 90 | 0.554 | 10.1 | 0.34 | 10.7 | 0.47 |
| C | 70 | 0.03 | 5.03 | 0.18 | 5.37 | 0.24 |

The $D_0$ is transformed by using the empirical relationship expressed by

$$D_0 = k_T M^{-B} \tag{17}$$

where $M$ is the molecular weight, $k_T$ is a proportionality constant, and $B$ reflects the hydrodynamic properties of the macromolecule. The values of $B$ are theoretically found to be $^1/_3$ for a hard sphere, $^1/_2$ for a random coil at Θ conditions, and 1 for a rod. As the area under the line width (and, therefore, the diffusion coefficient) distribution is proportional to the total scattered intensity, which is proportional to the integral $\int f(M)M^2P(\theta,M)\,dM$, the distribution axis is transformed through

$$f^*(M)\Delta M = G(D)\Delta D/M^2P(\theta,M) \tag{18}$$

where $f^*(M)$ is the unnormalized number distribution of the molecular weight, $\Delta M$ is the width of a segment in molecular weight space (eq 18 requires that the transformation be done in a piecewise fashion), $P(\theta,M)$ is the particle scattering factor for a scatterer of molecular weight $M$ at a scattering angle of $\theta$, and $\Delta D$ is the width of a segment in $D$ space. While $\Delta D$ is constant, $\Delta M$ is not, by virtue of the nonlinear transformation. Finally, we normalize $f^*(M)$ by

$$f(M)\Delta M = f^*(M)\Delta M/\sum f^*(M)\Delta M \tag{19}$$

Once $f(M)$ is computed, we may match $M_w$ by varying $k_T$. It is important to note that we must use an independently measured value of the molecular weight in order to provide a proper scale for the molecular weight axis. Although we have used the weight-average molecular weight $M_w$ for the determination of $k_T$, it is equally valid to use $M_n$ from osmometry or $M_z$ from sedimentation coefficient measurements. François et al.[14] have found

$$\langle r_g^2\rangle^{1/2} = 7.49 \times 10^{-2}M^{0.64} \quad (\text{Å}) \tag{20}$$

by making Zimm plots of fractionated samples, and we have used their exponent in eq 19. The particle scattering factor for random coils is used:

$$P(\theta,M) = (2/Q^2)\{\exp(-Q) + Q - 1\} \tag{21}$$

where $Q = K^2r_g^2$. The molecular weight dependence of $P(\theta,M)$ is explicitly related to $r_g$ via eq 20.

As mentioned previously, the starting form of $G(\Gamma)$ will influence the molecular weight transformation in a number of ways. The shape of the deduced $f(M)$ will not be noticeably altered, but values of measured parameters deduced from $f(M)$ will be affected. The fundamental reason lies in the nonlinear transformation (eq 17), which results in $\Delta M$ (eq 18) being very large at the high molecular weight end of $f(M)$. Since light scattering experiments measure properties that are weight averaged ($M_w$) or $z$ averaged ($\langle D\rangle_z$, $\langle r_g^2\rangle_z$), we need to pay particular attention to this distortion in $\Delta M$. Furthermore, the value of $P(\theta,M)$ must be computed as an average value over the segment we used for the transformation. At high molecular weights, $P(\theta,M)$ changes most rapidly. In the histogram approach, we use the step size of the histogram as the segment for the transformation and compute $M$ and $P(\theta,M)$ at the center of the segment. This practice may lead to a situation whereby the width of the highest molecular weight segment is greater than the sum of the widths of all other steps. It is for this reason that we have computed continuous forms of $G(\Gamma)$ in addition to the step form of the histogram technique. Using Pearson's form, we may make $\Delta M$ as small as necessary on the high molecular weight end of $f(M)$ in order to keep the error of $P(\theta,M) \lesssim 5\%$ from the center to the end of the transformation segment.

## V. Conclusions

The characteristics of each of the three forms of $G(\Gamma)$ we have used are summarized in Table VI in terms of the five requirements listed previously.

Point 6 of Table VI is perhaps misleading; we wish to emphasize that if one were to fit a bimodal distribution using the three approaches of $G(\Gamma)$, as well as the method of moments, only the histogram technique would show clearly a bimodal character. While the computational requirements of the simple form of $G(\Gamma)$ are appealing, we have not utilized this approach extensively. The qualified yes for point 2 for the simple form in Table VI reflects the fact that a two-parameter fit such as eq 11 cannot be expected to represent an arbitrary distribution as well as the Pearson distribution function, with four effective parameters. We must emphasize, however, that our purposes are to deduce $f(M)$ of a polymer sample that is quite polydisperse and, more importantly, has a long tail at the high molecular weight end of the distribution. For a narrow distribution with reasonable molecular weight cut-

Table VI
Comparison of Simple Form, Histogram, and Pearson Techniques

| | simple form | histogram[a] | Pearson |
|---|---|---|---|
| 1. form of $G(\Gamma)$ compatible with Laplace transformation | yes | no | no |
| 2. continuous distribution | qualified yes | no | yes |
| 3. regular trends and magnitude of error in deviation plot | ~10%, trends obvious | <1%, random | ~1%, random |
| 4. "correct" results for $\bar{\Gamma}$, $\mu_2/\bar{\Gamma}^2$, respectively | yes | yes, yes | yes, yes |
| 5. computational requirements | low CPU,[b] low PE[b] | moderate CPU, high PE | very large CPU, moderate PE |
| 6. a priori knowledge of $G(\Gamma)$ needed | yes | no | qualified yes |

[a] In the histogram method, we have used equal steps even though the Laplace transform suggests a more natural logarithmic step spacing. For very broad distributions, logarithmic spacing in Γ space tends to yield better results.
[b] CPU = computer time, PE = programmer expertise.

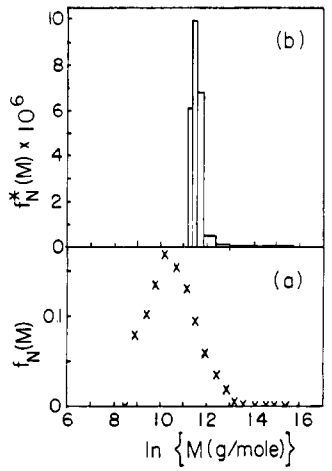


**Figure 11.** The number-average $f(M)$ for sample A ($C$ = 0.4 wt %) is shown as derived from a histogram fit of light scattering data ($\theta$ = 120°) in panel b. The GPC results are given in (a).

offs, we suspect that the simple form of $G(\Gamma)$ may be useful and is adequate for qualitative analysis. For a broader distribution with a sharp cutoff, the histogram technique would be appropriate. However, for the unimodal polyacrylamide distribution in question, which is certainly not uncommon, the more time-consuming Pearson fit yields the best results.

A direct comparison of the GPC-derived $f(M)$ and $f(M)$ obtained from the transformation of $G(\Gamma)$ is made in Figure 11 for sample A. The obvious discrepancy is caused by the fact that the light scattering data are heavily biased by larger particles, which is easily appreciated when we realize that the scattering power increases as the sixth power of the radius of the molecule. On the other hand, the larger molecules tend to pass through the GPC column quickly, without being separated efficiently. The ratio of $M_z/M_w$ indicates that from GPC, $M_n$:$M_w$:$M_z$ = 1:2:4, while from the histogram and the Pearson fits, we obtain $M_z/M_w$ = 1.6 and 2.5, respectively. We feel that when the higher molecular weight component is of interest, the light scattering $f(M)$ may be more relevant and useful.

## References and Notes

(1) Chu, B.; Gulari, Esin; Gulari, Erdogan *Phys. Scr.* **1979**, *19*, 476.
(2) Gulari, Esin; Gulari, Erdogan; Tsunashima, Y.; Chu, B. *J. Chem. Phys.* **1979**, *70*, 3965.
(3) Gulari, Erdogan; Gulari, Esin; Tsunashima, Y.; Chu, B. *Polymer* **1979**, *20*, 347.
(4) Chu, B.; Gulari, Esin *Macromolecules* **1979**, *12*, 445.
(5) Klein, J.; Conrad, K.-D. *Makromol. Chem.* **1980**, *181*, 227.
(6) Ehl, J.; Louchenx, C.; Reiss, C.; Benoit, M. *Makromol. Chem.* **1964**, *75*, 35.
(7) Koppel, D. E. *J. Chem. Phys.* **1972**, *57*, 4814.
(8) Selser, J. *Macromolecules* **1979**, *12*, 909.
(9) Gulari, E.; Chu, B. *Biopolymers* **1979**, *18*, 2943.
(10) DiNapoli, A.; Chu, B. *ACS Symp. Ser.* on polysaccharides, to be published.
(11) Erdélyi, A.; Magnus, F.; Oberhettinger, F.; Tricomi, F. C. "Tables of Integral Transforms"; McGraw-Hill: New York, 1954.
(12) Ralston, Wilf, "Mathematical Methods for Digital Computers"; Wiley: New York, 1967; Vol. II.
(13) Chu, B.; Nose, T. *Macromolecules* **1979**, *12*, 599.
(14) François, J.; Sarazin, D.; Schwartz, T.; Weill, G. *Polymer* **1979**, *20*, 969.

# Photodegradation of 1-Naphthyl Methacrylate–Butyl Methacrylate Copolymers in Benzene Solution. 2. Effect of Intramolecular Excimer Formation

**Sei-ichi Nishimoto, Kyohnosuke Yamamoto, and Tsutomu Kagiya***

*Department of Hydrocarbon Chemistry, Faculty of Engineering, Kyoto University, Sakyo-ku, Kyoto 606, Japan.* *Received January 19, 1982*

ABSTRACT: Photostationary-state and transient fluorescence characteristics of copolymers of 1-naphthyl methacrylate (1NMA) with butyl methacrylate (BMA) have been investigated in deaerated benzene solution at room temperature. Dilute solutions of poly(1NMA-*co*-BMA) showed both monomer and excimer fluorescence emissions. The quantum yield for excimer emission ($\Phi_D$) relative to that for monomer emission ($\Phi_M$) increased with increasing 1NMA content. $\Phi_M$ was approximately equal to the quantum yield for main-chain scission ($\Phi_{cs}$) whereas $\Phi_D$ varied in inverse proportion to $\Phi_{cs}$ throughout the entire range of 1NMA content. Time-resolved measurements of fluorescence decays in conjunction with the quantum yields enabled determination of a set of kinetic parameters for the photophysical and photochemical primary processes in poly(1NMA-*co*-BMA) in deaerated benzene solution. It is concluded that main-chain scission of poly(1NMA-*co*-BMA) occurs from the monomer fluorescence state of the side-chain 1-naphthyl chromophore, in competition with monomer emission, but hardly at all from the excimer fluorescence state.

Intramolecular excimer formation is a phenomenon observed commonly for a variety of polymers bearing fluorescent chromophores in the side chain.[1,2] A number of studies were accomplished by means of photostationary-state fluorometry to correlate intramolecular excimer formation with polymer structures,[3-8] properties of polymer solution,[9] micro-Brownian motion of a polymer chain in solution,[10,11] and energy migration along a polymer chain.[12-16] Recent time-resolved fluorometric studies have enabled characterization of the kinetics of intramolecular excimer formation and related photophysical processes in polymer systems.[17-22] Little attention has, however, been paid to the effect of intramolecular excimer formation on the photochemical reactions in a polymer chain.[23]

In the preceding paper in this series,[24] the photodegradation of copolymers of 1-naphthyl methacrylate (1NMA) with butyl methacrylate (BMA) in deaerated benzene solution was demonstrated to be affected markedly by the content of the 1NMA monomer unit. In this work, the photostationary-state and transient fluorescence characteristics of poly(1NMA-*co*-BMA) have been determined as a function of 1NMA content to clarify the relationship

0024-9297/82/2215-1180$01.25/0 